Quantum vacuum photon modes and repulsive Lifshitz–van der Waals interactions

Louis Dellieu,* Olivier Deparis, Jérôme Muller, Branko Kolaric, and Michaël Sarrazin†
Research Center in Physics of Matter and Radiation (PMR), Department of Physics, University of Namur, 61 rue de Bruxelles, B-5000 Namur, Belgium
(Received 8 May 2015; revised manuscript received 16 November 2015; published 10 December 2015)

The bridge between quantum vacuum photon modes and properties of patterned surfaces is currently being established on solid theoretical grounds. Based on these foundations, the manipulation of quantum vacuum photon modes in a nanostructured cavity is theoretically shown to be able to change the Lifshitz–van der Waals forces from attractive to repulsive regime. Since this concept relies on surface nanopatterning instead of chemical composition changes, it drastically relaxes the usual conditions for achieving repulsive Lifshitz–van der Waals forces. As a case study, the potential interaction energy between a nanopatterned polyethylene slab and a flat polyethylene slab with water as the intervening medium is calculated. Extremely small corrugation heights (<10 nm) are shown to be able to change the Lifshitz–van der Waals force from attractive to repulsive, the interaction strength being controlled by the corrugation height. This new approach could lead to various applications in surface science.

DOI: 10.1103/PhysRevB.92.235418 PACS number(s): 82.35.Lr, 34.20.Gj, 68.08.Bc

I. INTRODUCTION

Many fundamental aspects and practical issues in the physics of interfaces are related to controlling interactions between surfaces [1,2]. In his seminal article [3], De Gennes pointed out the importance of van der Waals and electrostatic forces in adsorption, adhesion, and wetting phenomena. Recently, it became obvious that controlling forces between macroscopic bodies or surfaces are crucial for a variety of applications such as mechanics of nanomachines, stability of colloids, and communication between biological cells [1,2,4,5].

The growing interest in nanoelectromechanical systems urges the scientific community to study in depth van der Waals and electrostatic interactions within nanostructured systems [6,7]. In particular, looking at nanostructures in the theoretical framework of dispersive (van der Waals) interactions turns out to be of great interest, bothfrom fundamental perspectives and for quantum based-technologies [8]. In order to understand the influence of surface corrugations on Lifshitz–van der Waals interactions between macroscopic bodies, many approaches have emerged, each one addressing specific corrugation geometries [7]. On one hand, additive methods, such as the proximity force approximation and the pairwise summation, appear to be the most employed when describing interactions between smooth corrugated surfaces at short and long separation distances, respectively [7,9]. On the other hand, when considering corrugated surfaces with small correlation lengths (of the order of the separation distance), nonadditive methods such as scattering or perturbative approaches are required in order to take into account diffraction and correlation effects which occur at the nanoscale [7,10]. However, it is noteworthy that refinements of the above-mentioned approaches have led to their progressive convergence for a specific corrugation size and shape [7].

This article focuses on small-correlation-length nanostructures with steep features. In this case, the assimilation of the surface corrugation to a graded effective refractive index layer is relevant [11–13] and allows simplifying greatly the application of nonadditive methods while still taking fully into account electrodynamical coupling between features as explained below. Motivated by recent theoretical [13–15] and experimental [16] studies, we introduce the novel concept of manipulating quantum vacuum photon modes at the sub-10-nm scale in order to turn Lifshitz–van der Waals interactions from attractive to repulsive.

The article is organized as follows. After this introduction (Sec. I), we present in Sec. II the theoretical framework used for the description of Lifshitz–van der Waals interactions and we explain our theoretical approach to calculate the interfacial energy in the case of steep nanocorrugated surfaces. The relevant approximation used to describe steep nanocorrugated surfaces is introduced and justified in Sec. III. In Sec. IV we report on computational results and discuss how sub-10-nm corrugations allow us to control quantum vacuum photon modes and, in this way, to turn the Lifshitz–van der Waals force from attractive to repulsive. Perspectives and general remarks are finally provided in Sec. V.

II. THEORETICAL APPROACH

Over the last decades, the Lifshitz–van der Waals approach of interfacial interactions in macroscopic systems has been widely investigated, both theoretically and experimentally [17–23]. Although usually attractive, the interaction potential energy may become repulsive if particular conditions are satisfied [24]. Let us first consider a body (1) interacting with a body (2) via an intervening medium (3) (Fig. 1). Let us also consider for the moment that each element of this macroscopic system has a planar geometry (for now body 2 is treated as a flat homogeneous slab) and is characterized by a dielectric function $\varepsilon(i\xi)$, where $i\xi$ is the imaginary angular frequency. It is well established that repulsive Lifshitz–van der Waals interactions between the two bodies can take place if

*louis.dellieu@unamur.be
†michael.sarrazin@unamur.be

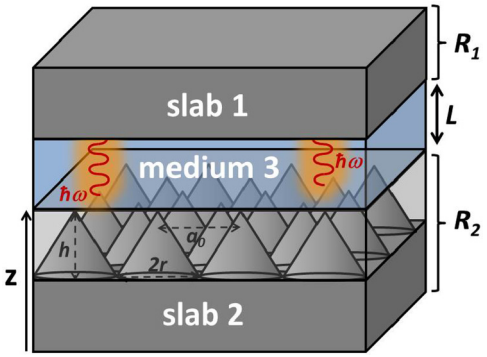

FIG. 1. (Color online) Bodies 1 and 2 interacting via an intervening medium 3. The two bodies are separated by a distance L. R_1 (R_2) is the Fresnel reflection coefficient of slab 1 (slab 2). The surface of body 2 is nanopatterned with corrugations that are described by a graded effective medium.

the following condition is satisfied [24]:

$$\varepsilon_1(i\xi) < \varepsilon_3(i\xi) < \varepsilon_2(i\xi), \tag{1}$$

where ε_i is the dielectric function of the ith component of the system. Equation (1) cannot be satisfied if the intervening medium is vacuum. Therefore, a liquid or a gas is needed to satisfy Eq. (1) for given slab materials [24]. Moreover, in practice, Eq. (1) imposes tight constraints on the choice of both the materials and the intervening medium, which makes the experimental observation of repulsive Lifshitz–van der Waals interactions challenging [25,26].

Hereafter, we introduce an original approach to modify Lifshitz–van der Waals interactions from a very different perspective, beyond the constraint set by Eq. (1). By tuning the virtual photon exchange between the two bodies, via nanopatterning of the surface of one of them (Fig. 1), it is possible to obtain a repulsive interaction potential energy, without any modification of the chemistry of materials, i.e., without changing their dielectric functions. The nature of the Lifshitz–van der Waals force—repulsive or attractive—is solely the result of controlling light-matter quantum interactions at the nanoscale.

The concept briefly described above is based on the fundamental interplay between physics of confined media and optical cavities. Here, the concept of confined space is applied to the particular geometry of a planar-like cavity [27–29] (Fig. 1). Actually, the present approach relies on the joined effects of electromagnetic (EM) confinement and surface patterning at the nanoscale, which are exploited to modify the interaction potential energy. In addition, since the studied system can be regarded as an optical cavity, it is possible to establish a formal link between optical properties of the cavity (quality factor Q, for instance) and Lifshitz–van der Waals forces between the slabs forming that cavity.

At the macroscopic level, the force, and thus the interaction potential energy, between two planar surfaces is related to the lowest (zero-point) energy state of the EM field, arising from the existence of virtual photons of energy $\frac{1}{2}\hbar\omega$ at all available frequencies which are exchanged between the two surfaces [7]. The interaction potential energy U can be written as [30] $U(L) = \frac{1}{2}\sum_k \hbar(\omega_k(L) - \omega_k(L \to \infty))$, where ω_k is the angular frequency of the kth vacuum photon mode available between the two surfaces separated by a length L (Fig. 1). $U(L)$ can then be easily related to the density of EM states $\rho(\omega, L)$ of the system such that $U(L) = \frac{1}{2}\hbar\int \omega(\rho(\omega,L) - \rho(\omega, L \to \infty))d\omega$. The quantity $\rho(\omega, L)$ can be obtained from classical electrodynamics.

The tuning of the zero-point energy is possible thanks to the presence of surfaces (boundaries), i.e., the presence of allowed modes of the EM field within the cavity [5,7]. Taking this fact into account, the force appears at the macroscopic level as the result of a manifold of vacuum photon modes occurring because the EM field must meet the appropriate boundary conditions at each surface. Moreover, these vacuum photon modes can be altered by patterning the surfaces [27], i.e., EM-field boundaries.

As explained above, the interaction potential energy considered in the present case results from the exchange of virtual photons between two interacting bodies. By summing the individual energies related to each mode available within the cavity, we can retrieve the total energy of the system from the photon density of states. Based on these arguments, we apply the so-called scattering approach [7] to calculate the interaction potential energy between two bodies facing each other. Accordingly, the interaction potential energy U is given by

$$U(L) = \frac{\hbar}{2\pi}\sum_{m=s,p}\int\frac{d^2k_{//}}{(2\pi)^2}\int_0^\infty d\xi \times \ln(1 - R_1^m(i\xi,\mathbf{k}_{//})R_2^m(i\xi,\mathbf{k}_{//})e^{-2\kappa L}), \tag{2}$$

where L is the separation distance between the bodies, $\kappa = \sqrt{\frac{\xi^2}{c^2} + |k_{//}|^2}$, R_1^m (R_2^m) is the generalized complex reflection coefficient of the first body (second body) in the m polarization state (s or p state), $k_{//}$ is the parallel component of the photon wave vector, and $i\xi$ is the imaginary angular frequency [31]. It is noteworthy that, in this method, the nanopatterned slab (here body 2) is treated as a graded effective medium (see [13] and discussion below).

For short separation distances ($L \leqslant 10$ nm), Eq. (2) is well approximated by the so-called Hamaker formula [32],

$$U(L) = -\frac{A_{132}}{12\pi L^2}, \tag{3}$$

where A_{132} is the effective Hamaker constant of the system, which can be deduced from the numerically computed energy, i.e., Eq. (2).

In the case where the intervening medium is vacuum, Eq. (2) appears to be efficient since it reproduces experimental results well [13]. In this case, using Eqs. (2) and (3), it is possible to retrieve the Hamaker constant A_{12} of the system [$A_{12} \equiv A_{132}$, where (3) is omitted when the intervening medium is vacuum]. Using the same procedure, it is also possible to retrieve the Hamaker constant A_{11} of the flat surface. The effective Hamaker constant A_{22} of the patterned surface, on the other hand, can be deduced indirectly from the well-known relation [2] $A_{12} = \sqrt{A_{11}}\sqrt{A_{22}}$ by using values of A_{12} and A_{11} calculated from Eqs. (2) and (3).

For numerical convenience [33,34], instead of computing A_{132} directly via Eq. (2) to obtain the interaction potential energy, we compute the effective Hamaker constant of the system [hereafter, (3) stands for fluid] from the well-known

relation [2,33,34]

$$A_{132} = (\sqrt{A_{11}} - \sqrt{A_{33}})(\sqrt{A_{22}} - \sqrt{A_{33}}), \quad (4)$$

where A_{ii} are the Hamaker constants of the corresponding media, which are obtained from the above-described procedure. The repulsive interaction potential energy is reached when A_{132} is negative [cf. Eq. (3)]. Therefore, according to Eq. (4), this condition is fulfilled when

$$A_{22} < A_{33} < A_{11}. \quad (5)$$

The condition imposed by Eq. (5) goes beyond the constraint set by Eq. (1). Indeed, when considering a nanopatterned surface, as in the present case, Eq. (1) cannot be used since dielectric functions are those of flat materials. On the other hand, Eq. (5) allows us to bypass this problem since the effective Hamaker constant of the nanopatterned surface can be calculated by the above-described procedure. Therefore, Eq. (5) has a more general application since it can be used simultaneously for both flat and nanopatterned surfaces.

III. MODELING AND SIMULATION DETAILS

Let us now develop the case of a practical two-body system consisting of two polyethylene (PE) slabs facing each other and separated by a distance L. In order to fulfill Eq. (5), we choose water (medium 3) as the intervening medium. It must be pointed out that such a configuration does not match Eq. (1). The first slab (slab 1) has a flat (planar) surface, while the second one (slab 2) is nanostructured, with cones of height h arranged on a hexagonal lattice with a lattice period chosen to be $a_0 = 10$ nm (Fig. 1). We choose a fixed cone base radius of $r = 5$ nm and a variable cone height h (ranging from 10 to 100 nm) in order to alter the optical properties of the surface. Indeed, such a geometry is known to improve the antireflection behavior of the surface, which in turns alters the vacuum photon modes of the system [13,35]. Moreover, since the PE surface is hydrophobic [1], we can assume a Cassie state [36] between water and the corrugated PE surface [13]. As a consequence, the void space between cones is filled by air, and water is localized above the top of the cones only.

At wavelengths below 20 nm, the PE permittivity is close to unity [37] and thus only vacuum modes above this spectral range are relevant. Since the lattice period is shorter than the relevant wavelength range, the patterned surface can be described by an effective material, i.e., an effective medium approach (EMA), with a graded permittivity $\varepsilon_{\text{eff}}(z)$ along its thickness such that

$$\varepsilon_{\text{eff}}(z) = 1 + (\varepsilon_{\text{PE}} - 1) f(z), \quad (6)$$

where ε_{PE} is the PE dielectric function, $f(z)$ is the filling fraction, given by $f(z) = \pi r(z)^2/S$ with $S = a_0^2\sqrt{3}/2$, and $r(z)$ is the radius of the circular section of the cones at coordinate z.

The use of the EMA has to be justified with great care. Indeed, this approximation usually requires the separation distance L to be equal to or larger than the lattice parameter a_0 of the periodically nanostructured surface [14]. The reason is that the distance is one of the main parameters determining the nature of the EM modes (radiative or evanescent) involved in the calculation of the Lifshitz–van der Waals interaction. In the case of a separation distance shorter than the lattice parameter, evanescent modes are dominant and are able to reproduce the details of the nanostructure, thereby invalidating the EMA [38,39]. However, in the present situation, the EMA remains valid for separation distances shorter than the lattice parameter. This nonintuitive result emerges from the weakness of the coupling between diffracted and specular orders due to both the optical properties of PE and the steepness of the corrugation (see Appendix A for a detailed justification of the use of the EMA).

The impact of the choice of water as the intervening medium has to be examined. Indeed, as a polar liquid, water induces an electrostatic double-layer at both surfaces facing each other, giving rise to an additional electrostatic repulsive force between them which, in experiments, could screen the Lifshitz–van der Waals repulsive force treated here. However, when considering the Cassie state regime, the electrostatic double-layer is located only on the top of the cones, which become steeper with increasing cone height. As a consequence, the electrostatic double-layer associated with the steep nanocorrugated PE surface becomes extremely small, leading to a dramatic decrease in the electrostatic repulsive interaction (see Appendix B). Therefore, in the present situation, the electrostatic repulsive interaction can be neglected compared to the Lifshitz–van der Waals interaction for any corrugation height.

The cornerstone of the present approach is related to the fact that tuning the antireflective properties of the bottom slab (thanks to nanocorrugations) allows us to tailor the virtual photon exchange within the cavity formed by the top flat PE slab and the bottom corrugated PE slab [13]. Since the presence of virtual photons causes dispersive interaction energy between slabs, it enables the control of the magnitude of attraction/repulsion between the two surfaces by only playing on the photon mode density inside the cavity.

IV. RESULTS AND DISCUSSION

As explained previously, the use of a fluid as the intervening medium left no choice but to compute the individual Hamaker

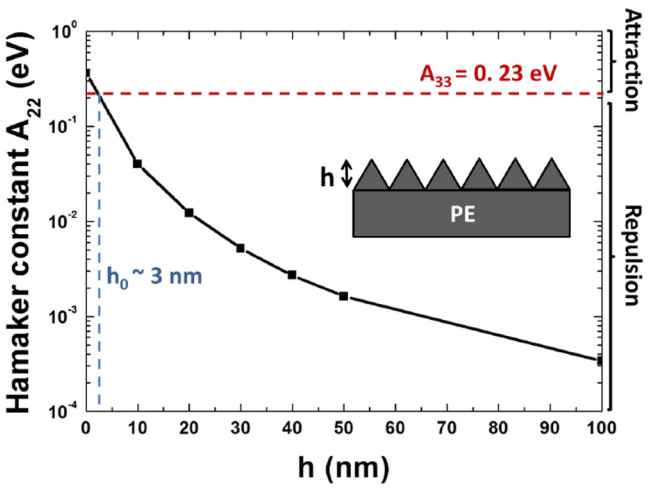

FIG. 2. (Color online) Hamaker constant A_{22} of a nanopatterned polyethylene slab (see inset) as a function of the cone height h.

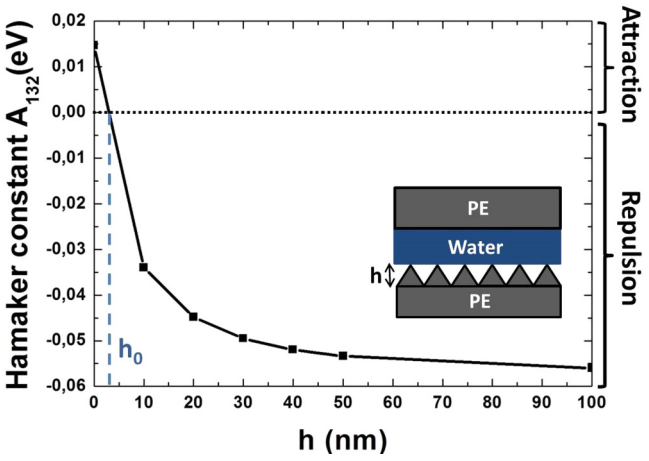

FIG. 3. (Color online) Hamaker constant A_{132} of a flat polyethylene (PE)/patterned PE system immersed in water (schematic in the inset) as a function of the cone height h.

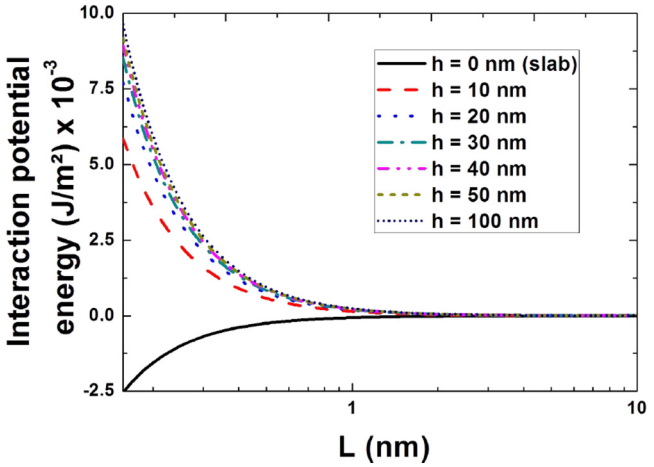

FIG. 4. (Color online) Interaction potential energy between PE slabs as a function of the cone height.

constants of each component of the system in the first step. We calculate from previously reported data [13] the effective Hamaker constant A_{22} of the corrugated PE slab using Eq. (2) and Eq. (3) for various cone heights (Fig. 2). Knowing the Hamaker constant A_{11} of a flat PE surface ($A_{11} = 0.36$ eV) [40] and the Hamaker constant A_{33} of water ($A_{33} = 0.23$ eV) [2], we then calculated the Hamaker constant A_{132} of the whole system from Eq. (4), as a function of the cone height (Fig. 3). A strong decrease in the Hamaker constant A_{132} with increasing cone height is observed, going from positive to negative values (Fig. 3). Here, the zero-crossing point for A_{132} takes place at $h_0 \approx 3$ nm. This critical point is reached when $A_{22} = A_{33}$ [dotted horizontal (red) line; Fig. 2], in accordance with the fact that a repulsive interaction is achieved only if Eq. (5) is satisfied. Therefore, the interaction potential energy becomes positive, i.e., a repulsive force (Fig. 4), for $h > h_0$ as soon as the Hamaker constant A_{132} of the system becomes negative (see [41]). It is noteworthy that, due to the small zero-crossing-point value h_0, it could be experimentally difficult to achieve a progressive transition from attractive to repulsive force while increasing the cone height (see [42] and [43]). Thus, observation of this progressive transition would require a higher h_0 value, which could be achieved by using flat materials with Hamaker constants A_{22} ($h = 0$) higher than the Hamaker constant A_{33} of the intervening medium (by at least one order of magnitude; see Fig. 2). Furthermore, owing to the Cassie-state regime of the present model, such materials are difficult to find [1]. Consequently, the transition from attractive to repulsive regimes cannot be easily observed or significantly modified (i.e., the h_0 value stays in the same range for most of the materials).

Such a dramatic modification of the dispersive energy of the system arises from the strong decrease in the Hamaker constant A_{22} of the nanopatterned PE slab as the cone height increases (note the logarithmic scale in Fig. 2). Phenomenologically, this result can be explained by the fact that the increase in the cone height h causes the decrease in the reflection coefficient of the nanopatterned PE slab $\mathcal{R}_2$. Consequently, the quality factor Q of the Fabry-Perot cavity also decreases [Fig. 5(a)] since [44]

$$Q = -2\pi \frac{1}{\ln(\mathcal{R}_1\mathcal{R}_2(1-\mathcal{A}_3)^2)} \frac{2L}{\lambda}, \tag{7}$$

where $\mathcal{R}_i = |R_i|^2$ and $\mathcal{A}_3$ is the optical absorption loss of the intervening medium (3) for a single path in the cavity (i.e., $\mathcal{A}_3$ is given by Beer-Lambert law). Moreover, the mean value of the quality factor $\langle Q \rangle$ was calculated by integration of Eq. (7) in the relevant spectral range, from 50 to 300 nm [Fig. 5(b)]. We observe a decrease in $\langle Q \rangle$ as the cone height increases, down to 49% of the initial value (i.e., for flat slabs) [Fig. 5(b)]. As Q decreases, the EM energy stored in the Fabry-Perot cavity is reduced [44]; i.e., the number of vacuum photon modes available within the cavity and that contribute to the interaction potential energy $U(L) \propto \sum_k \hbar\omega_k(L)$ diminishes. Therefore, the attractive behavior of the interaction potential energy becomes weaker while, owing to the geometry of the studied system and the choice of materials, the repulsive behavior becomes stronger. Overall, controlling the optical properties of the cavity enables us to tune the strength of the attractive/repulsive force. It is noteworthy that such an interpretation, although based on solid physical ground (i.e., the energy storage in an optical cavity), relies on a heuristic approach and still requires the establishment of a direct theoretical link between the quality factor and the Lifshitz–van der Waals interaction.

V. CONCLUSION

In conclusion, we have shown theoretically that extremely small and steep nanoscopic corrugations on the surface of one of two interacting bodies are able to turn Lifshitz–van der Waals interactions from attractive to repulsive, as well as to control the strength of the interactions by changing the corrugation height. The present approach is appealing since it offers the possibility of achieving a repulsive interaction only by nanopatterning one of the surfaces. Therefore, constraints with respect to the choice of materials [24–26] are relaxed. In the end, we are aware of the fact that an experimental proof of the concept is a very difficult task due to the engineering complexity related to the achievement of the pattern depth

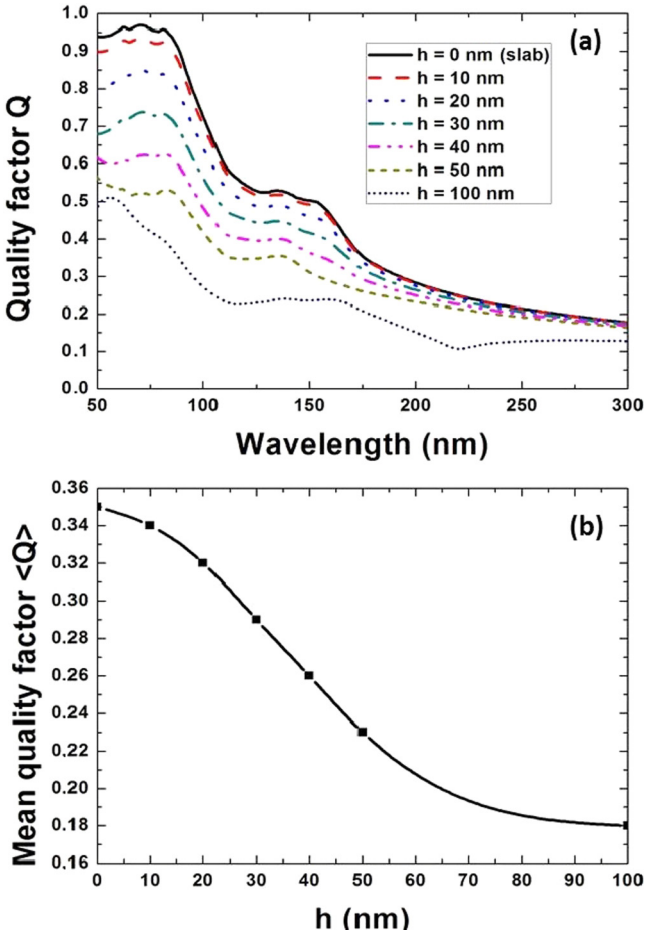

FIG. 5. (Color online) (a) Quality factor Q of the Fabry-Perot cavity formed by a flat polyethylene slab and a patterned polyethylene slab. Q is given vs the wavelength for various cone heights. (b) Mean value (integration over wavelength) of the quality factor of the cavity described above. Both slabs are separated by water.

of just a few nanometers. However, in the light of a recent experimental study [16], the presented concept could open new perspectives on the control of attractive/repulsive interactions by nanopatterning. Indeed, fabricated patterns could be used to control macroscopic interactions in a variety of applications, ranging from biology [45] to materials science, for controlling wettability, adhesion, and adsorption [1,2].

ACKNOWLEDGMENTS

L.D. was supported by the Belgian Fund for Industrial and Agricultural Research (FRIA). M.S. was supported by the Cleanoptic project (Development of Super-hydrophobic Anti-reflective Coatings for Solar Glass Panels/Convention No. 1117317) of the Greenomat program of the Wallonia Region (Belgium). B.K. acknowledges financial support from the Action de Recherche Concertée (BIOSTRUCT project) of the University of Namur (UNamur) and support from the Nanoscale Quantum Optics COST-MP1403 action. This research used resources of the "Plateforme Technologique de Calcul Intensif" (PTCI; http://www.ptci.unamur.be) located at UNamur, Belgium, which is supported by the FRS-FNRS. The PTCI is a member of the Consortium des Equipements de Calcul Intensif (CECI; http://www.ceci-hpc.be).

L.D. and M.S. contributed equally to this work.

APPENDIX A: JUSTIFICATION OF THE EFFECTIVE MEDIUM APPROACH

Although the EMA is fully relevant in optics when dealing with the far field, it could beargued that it is inappropriate for describing the near field, which plays a nontrivial role in the calculation of the interaction potential energy at short distances [46,47]. Indeed, the evanescent near field exhibits lateral fluctuations which are expected to mimic the surface corrugation [48]. Therefore, the EMA is *a priori* inappropriate in describing these fluctuations accurately. However, the careful analysis described below leads us to qualify this restriction in the specific case of subwavelength periodically patterned surfaces. The specular order couples with all the evanescent diffracted orders, which are all coupled together as well. As a result, they constitute the fluctuating near field. Let us formally examine such couplings in the theoretical framework of the rigorous coupled-wave analysis method [49]. The Fourier series expansion of the dielectric constant is written

$$\varepsilon(z,\rho) = \sum_{\mathbf{g}} \varepsilon_{\mathbf{g}}(z) e^{i\mathbf{g}.\rho}, \tag{A1}$$

where ρ denotes a real-space vector in the primitive cell with basis vectors $\mathbf{a_1}$ and $\mathbf{a_2}$ (Fig. 6), and $\mathbf{g}$ is a reciprocal lattice vector. By virtue of Floquet-Bloch theorem, the electric $\mathbf{E}$ and displacement $\mathbf{D}$ fields expand as

$$\mathbf{E}(z,\rho) = \sum_{\mathbf{g}} \mathbf{E}_{\mathbf{g}}(z) e^{i(\mathbf{g}+\mathbf{k}_{//}).\rho}, \tag{A2}$$

$$\mathbf{D}(z,\rho) = \sum_{\mathbf{g}} \mathbf{D}_{\mathbf{g}}(z) e^{i(\mathbf{g}+\mathbf{k}_{//}).\rho}. \tag{A3}$$

Since $\mathbf{D} = \varepsilon_0 \varepsilon(z,\rho)\mathbf{E}$, we can rewrite $\mathbf{D}_{\mathbf{g}}(z)$ as

$$\mathbf{D}_{\mathbf{g}}(z) = \sum_{\mathbf{g}'} \varepsilon_0 \varepsilon_{\mathbf{g},\mathbf{g}'} \mathbf{E}_{\mathbf{g}'}(z), \tag{A4}$$

where $\mathbf{g}'$ is another reciprocal lattice vector and the Fourier matrix element $\varepsilon_{\mathbf{g},\mathbf{g}'}$ expresses the coupling between diffracting orders $\mathbf{g}$ and $\mathbf{g}'$. When describing the cone by cylinder stack,

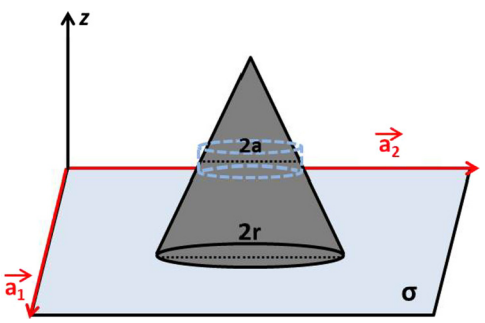

FIG. 6. (Color online) Primitive cell of the periodic patterned structure under study. In computations, the cone is described by a stack of cylinders of radius $a \in [0,r]$.

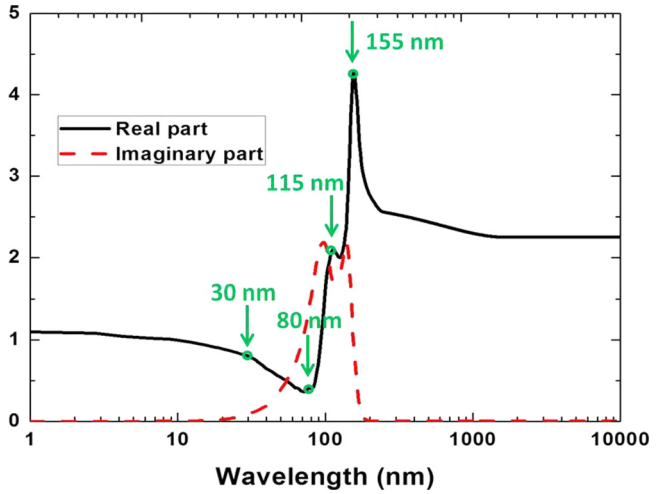

FIG. 7. (Color online) Dielectric function ε_s of polyethylene. Arrowed values are those used for numerical simulations (see Fig. 9).

$\varepsilon_{\mathbf{g},\mathbf{g}'}$ in a given layer is written as

$$\varepsilon_{\mathbf{g},\mathbf{g}'} = \varepsilon_m \delta_{\mathbf{g},\mathbf{g}'} + (\varepsilon_s - \varepsilon_m)\frac{2\pi a^2}{\sigma}\frac{J_1(|\,\mathbf{g}-\mathbf{g}'\,|\,a)}{|\,\mathbf{g}-\mathbf{g}'\,|\,a}, \qquad \text{(A5)}$$

where a is the cylinder radius at coordinate z (Fig. 6), J_1 is the first-order Bessel function, ε_m is the dielectric constant of the surrounding medium (here vacuum), ε_s is the dielectric constant of PE, $\delta_{\mathbf{g},\mathbf{g}'}$ is the Kronecker symbol, and σ is the primitive cell surface (Fig. 6). Due to the subwavelength size of the corrugation period, mode coupling [Eq. (A5)] gives rise to evanescent waves propagating along the surface.

Careful examination of Eq. (A5) indicates that the coupling constant $\varepsilon_{\mathbf{g},\mathbf{g}'}$ vanishes in two limit cases: (i) for low refractive index contrast, i.e., $\varepsilon_s \to \varepsilon_m$, and (ii) in the topmost layers where the cylinder radius a becomes very small and ultimately tends to 0 (note that $\lim_{a\to 0}\frac{J_1(|\mathbf{g}-\mathbf{g}'|a)}{|\mathbf{g}-\mathbf{g}'|a} = \frac{1}{2}$). As a consequence, in both limit cases, due to the extremely weak coupling, evanescent waves tend to vanish within the cavity. In the present study, limit case i is always reached at wavelengths equal to or shorter than 30 nm because of the dielectric properties of PE, i.e., $\mathrm{Re}(\varepsilon_s) \to 1$ and $\mathrm{Im}(\varepsilon_s) \to 0$ (Fig. 7). On the other hand, since evanescent waves propagate near the very top of the cones, and given the steepness thereof (i.e., $a \to 0$), limit case ii is always satisfied. These predictions need, however, to be verified by numerical simulations.

In order to probe the evanescent waves inside the cavity, we numerically simulated, by finite-difference time domain [50,51] homemade code, the diffracted field patterns which originate from oscillating dipoles inserted inside the cavity. These simulations model the EM field coming from quantum fluctuations inside the cavity. Both the actual three-dimensional structure [Fig. 8(a)] and its corresponding EMA description [Fig. 8(b)] were simulated using a cone height of 40 nm and a separation distance of 5 nm as an illustration. The EM responses to dipole excitation of both configurations were probed through normalized field intensity maps (Fig. 9). Maps are drawn for each computational cell (dashed lines in Fig. 8) and display only the diffracted field, i.e., with dipole radiation removed. The wavelengths of the radiating dipole

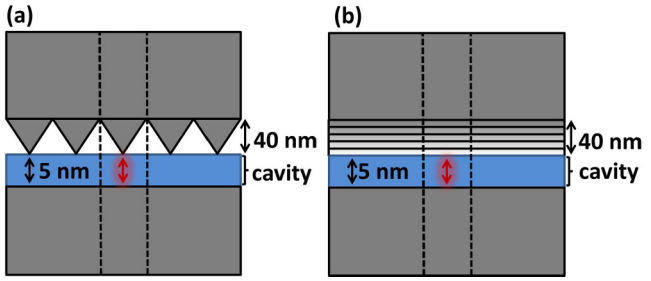

FIG. 8. (Color online) Sketches of the configuration used in finite-difference time-domain simulations for the cone array structure (a) and its corresponding EMA description (b). The lighter (red) arrow denotes an oscillating dipole and dashed lines show the limits of the computational cell. One dipole is inserted in each cell and periodically repeated.

(30, 80, 115, and 155 nm) were selected in order to sample the spectral range which is relevant to PE, according to its optical properties. At all these wavelengths except 30 nm, limit case i is not reached (Fig. 7) but limit case ii is reached near the top of the cones. In all cases, no significant differences are observed between the EM responses of the cone array structure and its EMA description (Fig. 9; relative error less than 2%). This result demonstrates that the fluctuations of the evanescent waves resulting from the coupling between diffracted orders

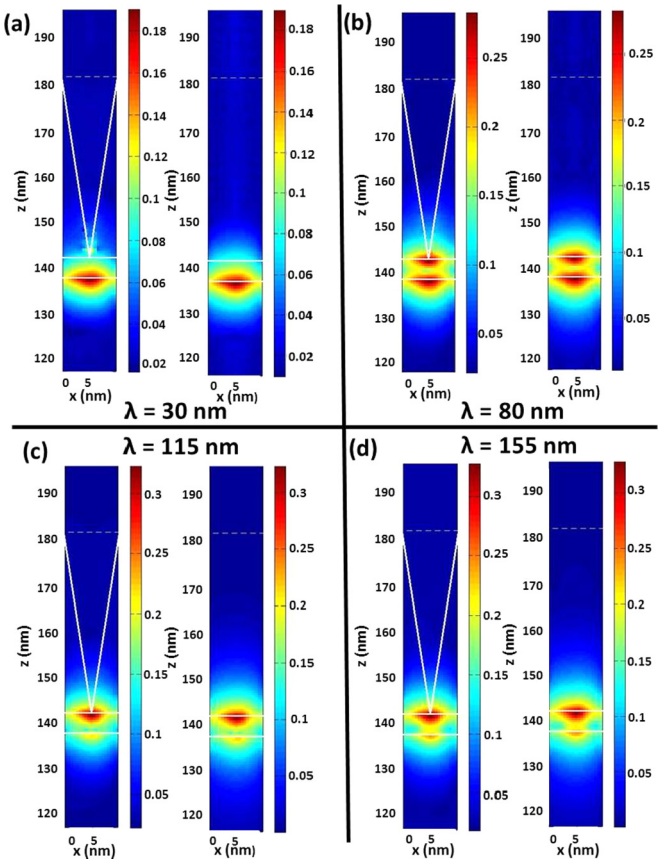

FIG. 9. (Color online) Maps of the normalized intensity of the diffracted field for different wavelengths in the three-dimensional structure (left plots) and its EMA description (right plots).

and specular orders are extremely weak, which therefore well justifies the use of the EMA in the present case.

Note that, for a cavity made of materials with mobile charges, surface plasmon polaritons would produce strongly modulated evanescent waves which would dominate Lifshitz–van der Waals interactions [47,52]. In this case, the EMA description would obviously fail. Since PE cannot support surface plasmon polaritons, the above-mentioned problem is excluded here.

In summary, the shallowness of evanescent wave fluctuations justifies the use of the EMA in the present situation. The underlying physical reason is the weak mode coupling due to both the optical properties of PE and the steepness of the corrugation. The use of a graded index profile for the EMA description turns out to be reliable in rendering these shallow fluctuations. In addition, the EMA avoids numerical stability issues while dealing with the direct computation of the scattering matrices of steep three-dimensional structures made of materials with low-contrast optical indexes, while computing the Lifshitz–van der Waals force. This is a considerable advantage of the proposed method.

APPENDIX B: ELECTROSTATIC POTENTIAL ENERGY CALCULATION

Here, we evaluate the relative contribution of electrostatic forces to the interfacial interaction in the case of PE slabs facing each other at a very small separation distance (around 10 nm). Let us first consider two flat surfaces facing each other and separated by a distance L with a liquid as the intervening medium. The electrostatic potential energy associated with the electrostatic double-layer formed at both surfaces is given by [1]

$$W(L) = \varepsilon_r \varepsilon_0 \kappa \left[2\psi_1\psi_2 e^{-\kappa L} - \left(\psi_1^2 + \psi_2^2\right) e^{-2\kappa L}\right], \quad \text{(B1)}$$

where ε_r is the static permittivity (dielectric constant) of the liquid, ε_0 is the vacuum permittivity, κ is the inverse of the Debye length of the liquid, and ψ_i is the surface potential of the ith surface.

Replacing now one of the two surfaces with a periodically nanostructured surface, here an array of cones, and using the Derjaguin approximation [1], the electrostatic potential energy is given by

$$W(L) = 2\pi \varepsilon_r \varepsilon_0 \tan^2(\alpha) e^{-\kappa L} \times \left[2\psi_1\psi_2 - (1/4)\left(\psi_1^2 + \psi_2^2\right) e^{-\kappa L}\right] / \kappa S, \quad \text{(B2)}$$

where α is the opening angle of the cone and $S = a_0^2\sqrt{3}/2$. It is noteworthy that the Derjaguin approximation is valid only if the Debye length of the liquid is smaller than the lattice period a_0 of the structured surface so that the electrostatic potential energy is not affected by coupling effects between cones.

In the case study presented in this article, the surface potential of both PE surfaces is equal to −30 mV [1], the static permittivity of water is equal to 78.2 J m^{-1} V^{-2} [1], and the Debye length of water is equal to 1.5 nm [1] (the Debye length of groundwater is used for more realistic considerations). Note that the value of the Debye length allows one to use Eq. (B2) since the correlation length (i.e., cone interdistance) is one order of magnitude larger. The electrostatic potential energy for various cone heights is shown in Fig 10. The results of this calculation are discussed in the article.

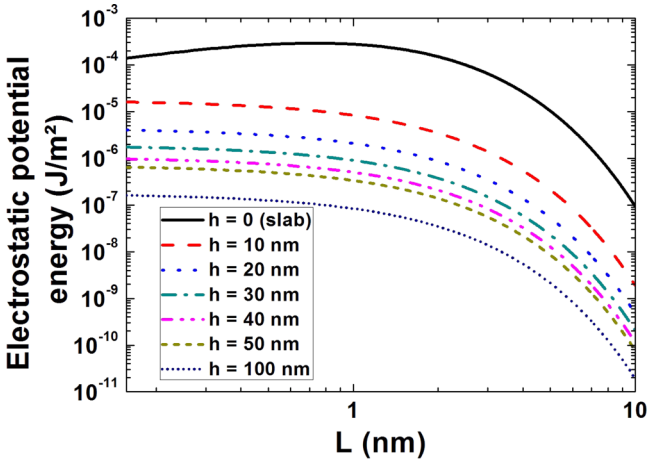

FIG. 10. (Color online) Electrostatic potential energy between polyethylene slabs as a function of cone height. Note the orders of magnitude on the y axis in comparison with Fig. 4.

[1] J. Israelachvili, *Intermolecular and Surface Forces* (Academic Press Elsevier, London, 2011).

[2] H.-J. Butt, K. Graf, and M. Kappl, *Physics and Chemistry of Interfaces* (Wiley-VCH, New York, 2003).

[3] P. G. de Gennes, Rev. Mod. Phys. **57**, 827 (1985).

[4] A. M. Alhambra, A. Kempf, and E. Martin-Martinez, Phys. Rev. A **89**, 033835 (2014).

[5] H. B. Chan, V. A. Aksyuk, R. N. Kleiman, D. J. Bishop, and F. Capasso, Science **291**, 1941 (2001).

[6] J. Yu, G. A. Rance, and A. N. Khlobystov, J. Mater. Chem. **19**, 8928 (2009).

[7] M. Bordag, G. L. Klimchitskaya, U. Mohideen, and V. M. Mostepanenko, *Advances in the Casimir Effect* (Oxford University Press, New York, 2009).

[8] H. J. Kimble, Nature **453**, 1023 (2008).

[9] W. Broer, G. Palasantzas, J. Knoester, and V. B. Svetovoy, Phys. Rev. B **85**, 155410 (2012).

[10] G. Palasantzas, V. B. Svetovoy, and P. J. van Zwol, Phys. Rev. B **79**, 235434 (2009).

[11] A. Gusso and U. B. Reis, Europhys. Lett. **99**, 36003 (2012).

[12] F. S. S. Rosa, D. A. R. Dalvit, and P. W. Milonni, Phys. Rev. A **78**, 032117 (2008).

[13] L. Dellieu, O. Deparis, J. Muller, and M. Sarrazin, Phys. Rev. Lett. **114**, 024501 (2015).

[14] A. P. McCauley, F. S. S. Rosa, A. W. Rodriguez, J. D. Joannopoulos, D. A. R. Dalvit, and S. G. Johnson, Phys. Rev. A **83**, 052503 (2011).

[15] N. Cherroret, R. Guerout, A. Lambrecht, and S. Reynaud, Eur. Phys. J. D **69**, 1 (2015).

[16] F. Intravaia, S. Koev, I. W. Jung, A. A. Talin, P. S. Davids,

R. S. Decca, V. A. Aksyuk, D. A. R. Dalvit, and D. Lopez, Nat. Commun. **4**, 2515 (2013).
[17] E. M. Lifshitz, Sov. Phys. JETP **2**, 73 (1956).
[18] A. Lambrecht, P. A. M. Neto, and S. Reynaud, New J. Phys. **8**, 243 (2006).
[19] G. L. Klimchitskaya, U. Mohideen, and V. M. Mostepanenko, Rev. Mod. Phys. **81**, 1827 (2009).
[20] B. Geyer, G. L. Klimchitskaya, and V. M. Mostepanenko, Phys. Rev. B **81**, 245421 (2010).
[21] P. J. van Zwol and G. Palasantzas, Phys. Rev. A **81**, 062502 (2010).
[22] P. J. van Zwol, G. Palasantzas, and J. T. M. De Hosson, Phys. Rev. B **79**, 195428 (2009).
[23] P. J. van Zwol, G. Palasantzas, and J. T. M. DeHosson, Phys. Rev. E **79**, 041605 (2009).
[24] I. E. Dzyaloshinskii, E. M. Lifshitz, and L. P. Pitaevskii, Sov. Phys. Usp. **4**, 153 (1961).
[25] J. N. Munday, F. Capasso, and V. A. Parsegian, Nature **457**, 170 (2009).
[26] S.-W. Lee and W. M. Sigmund, Colloids Surf. A Physicochem. Eng. Aspects **204**, 43 (2002).
[27] B. Kolaric, H. Vandeparre, S. Desprez, R. A. L. Vallee, and P. Damman, Appl. Phys. Lett. **96**, 043119 (2010).
[28] M. Trupke, E. A. Hinds, S. Eriksson, E. A. Curtis, Z. Moktadir, E. Kukharenka, and M. Kraft, Appl. Phys. Lett. **87**, 211106 (2005).
[29] S. M. Dutra, *Cavity Quantum Electrodynamics: The Strange Theory of Light in a Box* (Wiley, Hoboken, NJ, 2005).
[30] D. Dalvit, P. Milonni, D. Roberts, and F. da Rosa, *Casimir Physics*. *Lecture Notes in Physics* (Springer-Verlag, Berlin, 2011).
[31] F. Intravaia and R. Behunin, Phys. Rev. A **86**, 062517 (2012).
[32] H. C. Hamaker, Physica (Amsterdam) **4**, 1058 (1937).
[33] J. Visser, Adv. Colloid Interface Sci. **15**, 157 (1981).
[34] J. Visser, Adv. Colloid Interface Sci. **3**, 331 (1972).
[35] D. G. Stavenga, S. Foletti, G. Palasantzas, and K. Arikawa, Proc. Biol. Sci. **273**, 661 (2006).
[36] A. B. D. Cassie and S. Baxter, Trans. Faraday Soc. **40**, 546 (1944).
[37] J. Ashok, P. L. H. Varaprasad, and J. R. Birch, in *Handbook of Optical Constants of Solids II*, edited by E. D. Palik (Academic Press Elsevier, New York, 1991).
[38] R. Zhao, J. Zhou, Th. Koschny, E. N. Economou, and C. M. Soukoulis, Phys. Rev. Lett. **103**, 103602 (2009).
[39] A. P. McCauley, R. Zhao, M. T. H. Reid, A. W. Rodriguez, J. Zhou, F. S. S. Rosa, J. D. Joannopoulos, D. A. R. Dalvit, C. M. Soukoulis, and S. G. Johnson, Phys. Rev. B **82**, 165108 (2010).
[40] C. J. Drummond and D. Y. C. Chan, Langmuir **13**, 3890 (1997).
[41] The results are presented in Fig. 4 for separation distances equal to or shorter than the lattice parameter. Nevertheless, we checked that the same behavior of the interaction potential energy (i.e., transition from attractive to repulsive regimes) was obtained for separation distances larger than the lattice parameter.
[42] Having a perfectly flat interface is not experimentally achievable [43]. However, the experimentally observed deviations from the perfectly flat interface do not affect the concept presented here. Indeed, the Hamaker constant of a nanopatterned surface is modified at the global level only if the pattern exhibits short correlation length corrugations [13]. Because the experimentally observed roughness occurs at long correlation lengths, the Hamaker constant of the ideally flat surface (in reality, rough) is not affected.
[43] R. Todorov, J. Tasseva, V. Lozanova, A. Lalova, T. Iliev, and A. Paneva, Adv. Condens. Matter Phys. **2013**, e308258 (2013).
[44] B. E. A. Saleh and M. C. Teich, *Fundamentals of Photonics*, 2nd ed. (Wiley-Interscience, New York, 2007).
[45] Y. Liu and Q. Zhao, Biophys. Chem. **117**, 39 (2005).
[46] Y. Zheng and A. Narayanaswamy, Phys. Rev. A **89**, 022512 (2014).
[47] F. Intravaia and A. Lambrecht, Phys. Rev. Lett **94**, 110404 (2005).
[48] D. Courjon, *Near-Field Microscopy and Near-Field Optics* (Imperial College Press, London, 2003).
[49] J. P. Vigneron, F. Forati, D. Andre, A. Castiaux, I. Derycke, and A. Dereux, Ultramicroscopy **61**, 21 (1995).
[50] A. Taflove and S. Hagness, *Computational Electrodynamics*, 3rd ed. (Artech House, Boston, 2005).
[51] J. Muller, G. Parent, G. Jeandel, and D. Lacroix, J. Opt. Soc. Am. A **28**, 868 (2011).
[52] H. Raether, in *Springer Tracts in Modern Physics*, edited by G. Hohler and E. A. Nickisch (Springer, Berlin, 1988), Vol. 111.